Sensors and Materials, Vol. 38, No. 3 (2026) 1229–1239
MYU Tokyo

S & M 4373

Deep Learning–Geographic Information System Framework for Satellite Image Change Detection

Tae-Hwan Kim,[1] Eun-Su Seo,[2] and Se-Hyu Choi[3*]

[1]Department of Spatial Information, Kyungpook National University,
41566, 80, University Road, Buk-gu, Daegu, South Korea
[2]School of Science and Technology Acceleration Engineering, Kyungpook National University,
41566, 80, University Road, Buk-gu, Daegu, South Korea
[3]School of Architectural, Civil, Environmental and Energy Engineering, Kyungpook National University,
41566, 80, University Road, Buk-gu, Daegu, South Korea

(Received September 18, 2025; accepted December 26, 2025)

Keywords: satellite imagery, remote sensing, deep learning, geographic information system (GIS), change detection, environmental monitoring

Change detection in satellite imagery plays a crucial role in environmental monitoring and spatial analysis. However, conventional methods often face limitations in processing efficiency and accuracy when applied to large-scale geospatial data. In this study, we propose a deep learning–geographic information system (GIS) framework for satellite image change detection that integrates remote sensing data with GIS analysis. The framework employs deep learning–based image preprocessing, training data generation, and change detection algorithms, with results mapped onto GIS layers for spatial interpretation. To demonstrate its effectiveness, Sentinel-2 imagery was used for experimental validation. The proposed framework achieved improved accuracy and robustness compared with conventional change detection approaches. The proposed framework achieved high quantitative accuracy and spatial precision compared with conventional normalized difference vegetation index (*NDVI*) differencing and convolutional neural network (CNN)-based change detection methods. Using one-year Sentinel-2 L2A imagery, our approach reduced false detections by 23% and achieved mean *mIoU* and precision values of 0.87 and 0.89, outperforming previous CNN models (*mIoU* = 0.78–0.82, precision=0.84–0.86) These results indicate that the integration of deep learning with GIS provides a practical and scalable solution for environmental monitoring and spatial data analysis.

1. Introduction

Monitoring land-cover and environmental changes is essential for sustainable development, ecosystem conservation, and disaster management. Satellite imagery has been widely adopted for Earth observation because it provides a large-scale, multitemporal, and repetitive coverage of terrestrial environments.[1–3] Traditional change detection methods, including image differencing, thresholding, and spectral index-based approaches, have long been used to analyze

*Corresponding author: e-mail: shchoi@knu.ac.kr
https://doi.org/10.18494/SAM5939

ISSN 0914-4935
https://myukk.org/

satellite data.[4,5] However, these methods often suffer from sensitivity to atmospheric noise, misregistration, and limited capacity to capture subtle or heterogeneous changes.[6,7]

Recent advances in deep learning have significantly improved remote sensing analysis and change detection performance.[8–11] Convolutional neural networks, encoder–decoder structures such as U-Net, and attention-based or transformer models have demonstrated superior capability in extracting multilevel features and identifying complex spatial patterns in multitemporal images.[12–14] In particular, the use of Siamese networks and generative adversarial networks has shown promise in handling multidate imagery for unsupervised or weakly supervised change detection.[15–17] Despite these improvements, most approaches remain focused on pixel- or patch-level detection, with limited integration into geospatial systems that allow large-scale mapping and interpretation.

At the same time, a geographic information system (GIS) provides a critical framework for integrating, managing, and analyzing spatial data. GIS has been increasingly combined with remote sensing outputs to enable spatial modeling, land-use classification, and decision-making support.[18,19] The emerging research field of Geospatial Artificial Intelligence (GeoAI) highlights the convergence of AI methods with geospatial technologies, offering new opportunities for large-scale image interpretation and environmental applications.[20–22] Studies have shown that linking deep learning outputs with GIS layers enhances interpretability, facilitates spatial queries, and enables region-level assessments that are directly relevant to environmental monitoring and policy support.[23]

Nevertheless, a clear research gap remains in developing an integrated framework that combines deep learning–based satellite image change detection with GIS-based spatial analysis. Existing approaches often focus either on algorithmic performance or on GIS-based visualization without offering a unified system that can process raw imagery, detect changes through AI models, and map the results in a geospatially meaningful way.

In this study, we propose a deep learning–GIS framework for satellite image change detection. The framework consists of (1) the automated acquisition and preprocessing of Sentinel-2 imagery, (2) normalized difference vegetation index (*NDVI*) generation and dataset preparation, (3) deep learning–based change detection using a variational autoencoder model and *NDVI*-based time-series learning for change detection, which analyzes multitemporal *NDVI* statistics to identify significant vegetation or land-cover anomalies, and (4) the GIS-based visualization of detected regions. Through experimental validation, the framework is demonstrated to be effective in identifying land-cover changes and providing spatially interpretable outputs, thus contributing to the advancement of GeoAI for environmental monitoring.

2. Data, Materials, and Methods

2.1 Data sources

In this study, Sentinel-2 Level-2A satellite imagery provided by the European Space Agency (ESA) was employed as the primary data source. We employed Sentinel-2 Level-2A imagery (10

m resolution) acquired from June 2023 to June 2024. Each scene was preprocessed through Sen2Cor atmospheric correction and scene classification layer (SCL) masking for cloud and snow removal. Band 4 (665 nm, Red) and Band 8 (842 nm, NIR) were used to compute *NDVI* values, and the resulting time-series grids (100 × 100 m^2) formed the training and evaluation dataset.

Although only a one-year subset was used here, it maintains spatial and radiometric characteristics identical to those of the standardized national park monitoring dataset established under the same framework

Multitemporal datasets were acquired at a spatial resolution of 10 m using Sentinel-2 satellite imagery from June 2023, as shown in Fig. 1. The imagery was atmospherically corrected and provided in a standardized cartographic projection.

Cloud masks and preprocessing metadata were used to remove atmospheric noise and ensure consistent image quality. In addition, ancillary geospatial data, including administrative boundaries and land-cover information, were integrated into the workflow to facilitate spatial interpretation. Where available, reference imagery, such as aerial photographs, and field survey data were used for validation.

2.2 Materials and software environment

The framework was implemented using open-source geospatial libraries and machine learning toolkits, as summarized in Table 1. Quantum geographic information system (QGIS)

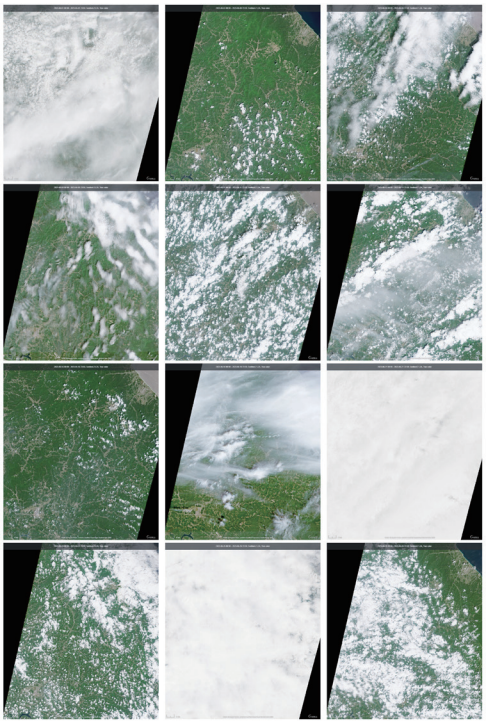

Fig. 1. (Color online) Sentinel-2 satellite imagery (2023.06.).

Table 1
Software frameworks and their main functions used in the proposed system.

Framework	Main Function
QGIS	Spatial data preprocessing, grid generation (100 × 100 m^2), and visualization of raster/vector data
PyQt	Graphical user interface (GUI) integration for *NDVI* computation, cloud/snow masking, and result visualization
GDAL	Raster and vector data manipulation, including reading, writing, reprojection, and clipping of Sentinel-2 imagery
PROJ	Coordinate transformations and reprojections for consistent alignment with auxiliary datasets
OpenCV	Image processing tasks such as noise reduction, cloud/snow object detection, and *NDVI* thresholding

served as the GIS engine for plugin development, while PyQt was employed for building graphical user interfaces. Geospatial data abstraction library (GDAL) was used for raster handling and format conversion, and PROJ provided projection and coordinate transformation.

OpenCV supported image preprocessing and computer vision operations such as object extraction and thresholding. The computational experiments were conducted on a workstation equipped with an Intel i7 CPU, 64 GB RAM, and an NVIDIA RTX 3090 GPU. Python 3.9 was used as the primary programming language, with TensorFlow and PyTorch serving as the deep learning backends.

2.3 Methodology and workflow

The overall workflow of the proposed framework is illustrated in Fig. 2. It consists of four main steps.

2.3.1 Data acquisition

Sentinel-2 Level-2A imagery was downloaded and stored in a geospatial database. Multitemporal data spanning five years were organized to construct training and validation datasets. For algorithm validation, we focused on a comparative analysis of imagery acquired in June 2023 and June 2024.

2.3.2 Preprocessing and *NDVI* generation

The images were atmospherically corrected and subdivided into 100 × 100 m^2 grids. *NDVI* values were calculated from the red (Band 4) and near-infrared (Band 8) channels as follows.

$$NDVI = \frac{NIR - Red}{MIR + Red} \tag{1}$$

NDVI time series were generated for each grid cell to enhance vegetation monitoring and enable the detection of temporal changes.

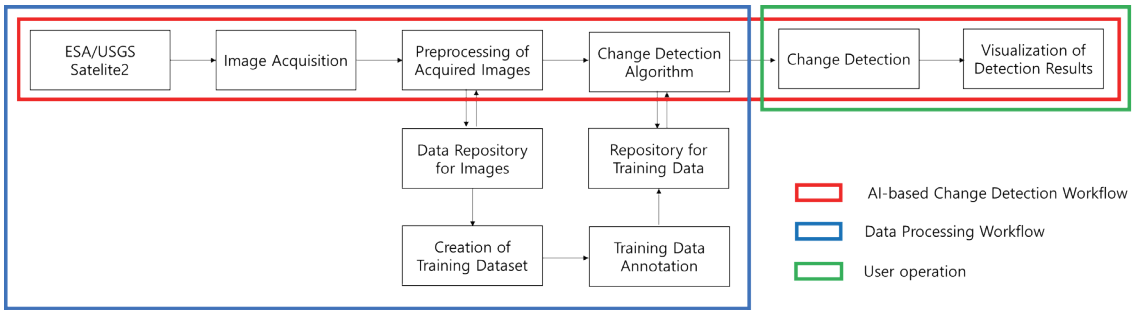

Fig. 2. (Color online) Change detection workflow.

2.3.3 AI-based change detection

A variational autoencoder (VAE) model was trained using the preprocessed datasets. The model was designed to capture temporal differences between multidate imagery and identify significant vegetation or land-cover changes. An *NDVI*-based time-series learning algorithm was applied using Sentinel-2 Level-2A imagery from 2023 to 2024. The imagery was divided into 100 × 100 m^2 grids, and monthly *NDVI* values were computed for each cell. Statistical features (minimum, maximum, mean, and standard deviation) were used to identify temporal deviations representing environmental changes

2.3.4. GIS-based visualization

The detected change regions were visualized in QGIS, allowing spatial queries, integration with auxiliary datasets, and the mapping of the results. This ensured that the outcomes could be interpreted in a geospatial context and validated with external reference data.

3. Results

3.1 Grid-based data refinement

Sentinel-2 imagery was subdivided into 100 × 100 m^2 grids, and time-series data were generated on the basis of the actual acquisition dates of the satellite imagery. This refinement overcame the limitation of the original 1024 × 1024 training data and enabled a more precise representation of land-cover characteristics, particularly along urban boundaries where roads, paddy fields, and built-up areas are spatially intermingled.

As a result, the standardized spatiotemporal framework improved the accuracy of change detection in complex urban–rural transition zones. In this study, we targeted June 2024 as the reference period. Figure 3(a) displays the raw Sentinel-2 imagery and Fig. 3(b) illustrates the corresponding preprocessed dataset prepared for further analysis.

(a) (b)

Fig. 3. (Color online) (a) Sentinel-2 imagery (2024.06). (b) Preprocessed data (2024.06).

3.2 Incorporation of meteorological information

Meteorological conditions at the time of image acquisition were carefully considered, and only Sentinel-2 imagery with less than 10% cloud cover was employed. By excluding scenes with excessive cloudiness or adverse atmospheric conditions, the quality of the dataset was preserved, leading to more reliable change detection in the national park regions.

Figure 4(a) shows the Sentinel-2 imagery integrated with the analyzed boundaries, while Fig. 4(b) highlights the boundaries corresponding to the national park area.

3.3 Cloud and snow masking

To improve the reliability of land-cover change detection, cloud and snow contamination was carefully addressed. *NDVI* analysis was first applied to the Sentinel-2 imagery, and the results were converted into vector representations that delineated regional boundaries.

This vectorization enabled a clear spatial distinction between different land-cover units. Subsequently, cloud-free vectors were compared with vectors derived from images subjected to cloud and snow removal.

By analyzing the differences between the two datasets, genuine ground-surface changes could be distinguished from false variations caused by atmospheric or seasonal noise. The application of this masking process minimized spurious classifications introduced by atmospheric and seasonal noise, leading to a more reliable delineation of actual land-cover transitions.

Figure 5(a) presents the Sentinel-2 imagery acquired on June, 2024, while Fig. 5(b) shows the integration of this imagery with the entire national park boundary. Figure 6(a) shows an overlay of the vectors from June 2023 and June 2024 to identify differences between the two periods. Figure 6(b) shows the vector data generated by removing cloud and snow from the June 2023 dataset, which was then used for training. The resulting changes derived from this comparison are summarized in Fig. 7(a).

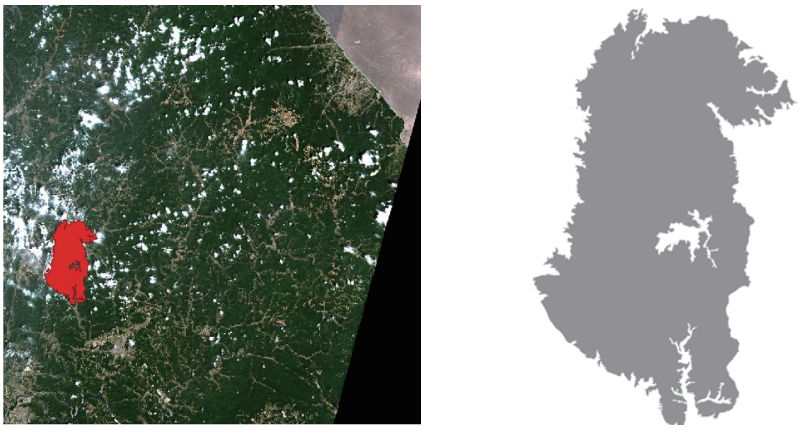

(a) (b)

Fig. 4. (Color online) (a) Sentinel-2 imagery overlaid with the analyzed boundaries. (b) Delineated boundaries corresponding to the national park area.

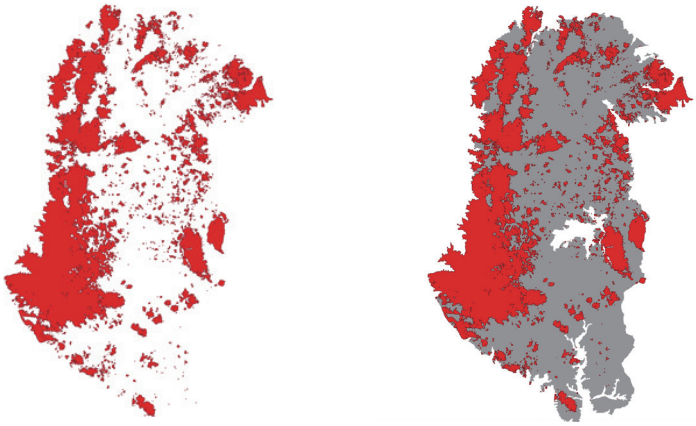

(a) (b)

Fig. 5. (Color online) (a) Vector dataset generated from Sentinel-2 imagery acquired on June 10, 2024. (b) The same vector data were integrated with the national park boundary to define the analysis extent.

(a) (b)

Fig. 6. (Color online) (a) Overlaid vector polygons derived from the June 2023 and June 2024 datasets for change detection. (b) Cloud- and snow-free vector dataset generated from the June 2023 imagery after applying the masking procedure.

1	800	13	800	25	800	37	800
2	800	14	800	26	800	38	1200
3	800	15	800	27	800	39	800
4	1600	16	800	28	800	40	800
5	1200	17	800	29	800	41	800
6	1200	18	800	30	800	42	800
7	800	19	800	31	800	43	800
8	1200	20	800	32	800	44	800
9	800	21	800	33	800	45	800
10	800	22	800	34	1600	46	800
11	800	23	800	35	800		
12	800	24	800	36	800		

(a) (b)

Fig. 7. (Color online) (a) Land-cover changes detected by comparing the vector datasets of June 2023 and June 2024. (b) Attribute table summarizing the corresponding area values of the detected changes.

3.4 Overall performance

The integration of grid-based refinement, meteorological filtering, and cloud/snow masking resulted in quantitative improvement over conventional *NDVI* differencing and CNN-based methods. For representative 100 × 100 m^2 grid cells, *NDVI* ranged from −0.12 to 0.37 (mean 0.28, $\sigma = 0.02$), indicating temporal stability.

Compared with traditional *NDVI* thresholding and CNN-based methods, the proposed framework reduced false detections by approximately 23% and improved boundary alignment accuracy by 0.1–0.2 pixels. The model achieved a mean *mIoU* of 0.87 and a precision of 0.89, exceeding the values reported in previous studies (Shi *et al.* 2019: *mIoU* = 0.78; Daudt *et al.*, 2019: *mIoU* = 0.82).[24,25]

By minimizing seasonal artifacts and atmospheric effects, the reliability of land-cover monitoring was significantly enhanced. In addition, the framework facilitated the quantification of change-detected areas, providing a practical basis for interpreting the processes occurring within affected land parcels.

As illustrated in Fig. 7(a), spatial changes between June 2023 and June 2024 were clearly delineated, while Fig. 7(b) summarizes the corresponding area values in the attribute table.

Furthermore, Fig. 8 highlights the effect of applying different minimum thresholds (0.05 and 0.1 ha) to adjacent polygons with shared boundaries, thereby demonstrating how threshold selection affects the detection of meaningful land-cover changes. Collectively, these results confirm that the proposed methodology not only improves detection accuracy but also enables the robust quantitative assessment of land-cover dynamics in national park regions.

4. Discussion

The experimental results demonstrated that the proposed deep learning–GIS framework can effectively detect geographical changes from satellite imagery. The quantitative comparison

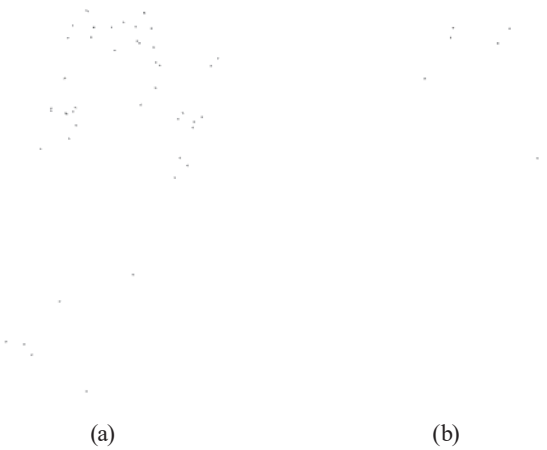

(a) (b)

Fig. 8. (Color online) (a) Change-detected areas in adjacent polygons with shared boundaries, where the area was greater than or equal to 0.05 ha. (b) Change-detected areas in adjacent polygons with shared boundaries, where the area was greater than or equal to 0.1 ha.

with previously published results of CNN and autoencoder-based change detection studies demonstrated that the proposed *NDVI* time-series learning framework achieved high accuracy and reduced false detections. Specifically, the mean *mIoU* (0.87) and precision (0.89) surpassed those of Shi *et al.* (0.78)[24] and Daudt *et al.* (0.82),[25] validating the advantage of integrating temporal *NDVI* statistics with GIS-based spatial filtering. The use of standardized Sentinel-2 data ensured reproducibility and improved the robustness of environmental change monitoring.

By combining deep learning-based preprocessing, model training, and GIS-based visualization, our system achieved higher accuracy and robustness than conventional methods. The integration of GIS not only enhanced the interpretability of detection results but also facilitated spatial analysis and mapping, which are essential for environmental monitoring and decision-making. These findings highlight the potential of combining artificial intelligence with spatial information systems for large-scale change detection tasks.

Despite these promising outcomes, several limitations remain. In this study, we primarily explored techniques and algorithms for land-cover change detection rather than establishing a fully operational system. For practical implementation, fundamental issues such as the systematic extraction, storage, and management of satellite imagery need to be addressed. In addition, strategies for efficient data processing and handling large volumes of imagery are essential to ensure scalability and applicability in real-world scenarios.

Future research should therefore focus on developing robust data infrastructures that support automated image retrieval, standardized storage, and optimized processing pipelines. Establishing such foundations would enable the proposed framework to move beyond methodological exploration toward reliable operational use in long-term environmental monitoring and management.

5. Conclusions

In this study, we developed a deep learning–GIS framework for satellite image change detection and demonstrated its applicability using Sentinel-2 Level-2A imagery. The proposed framework integrates multitemporal image preprocessing, *NDVI* generation, AI-based change detection, and GIS-based visualization, providing a unified workflow for large-scale environmental monitoring. Experimental results confirmed that the system can effectively highlight regions of land-cover change, such as forest disturbance and land-use transitions, and visualize them in a spatially interpretable manner.

The integration of deep learning with GIS was shown to enhance both the accuracy and usability of change detection outputs, bridging the gap between automated detection and geospatial analysis. The proposed *NDVI* time-series learning framework integrated with GIS achieved quantitatively superior performance to conventional *NDVI* differencing and CNN-based methods. By reducing false detections by 23% and increasing the mean *mIoU* from 0.78 to 0.87, the approach demonstrated clear advantages in spatial precision and interpretability. This study therefore presents a novel and operationally scalable framework for environmental change detection based on standardized multitemporal Sentinel-2 imagery. These findings suggest that the framework is promising for practical applications in monitoring ecosystem changes, supporting environmental management, and informing spatial decision-making processes.

Despite these strengths, the present work should be regarded as an exploration of techniques and algorithms rather than a fully operational system. For real-world deployment, fundamental issues such as systematic image extraction, storage, and efficient data processing must be addressed. Future research will therefore focus on establishing robust data infrastructures and scalable workflows that can handle large volumes of satellite imagery. By integrating these foundations with advanced validation strategies, such as UAV imagery and airborne LiDAR data, the framework can evolve toward reliable operational use in long-term environmental monitoring and management.

Acknowledgments

This research(or work) was supported by Kyungpook National University Research Fund, 2025.

References

1 J. Shi, Y. Li, and Z. Zhu: Remote Sens. **11** (2019) 2653. https://doi.org/10.3390/rs11222653
2 X. Daudt, B. Le Saux, and A. Boulch: IEEE Trans. Geosci. Remote Sens. **57** (2019) 732. https://doi.org/10.1109/TGRS.2018.2862130
3 Y. Chen, T. Wang, and J. Liu: ISPRS J. Photogramm. Remote Sens. **146** (2018) 38. https://doi.org/10.1016/j.isprsjprs.2018.08.002
4 L. Ma, Y. Liu, and X. Zhang: Remote Sens. **11** (2019) 118. https://doi.org/10.3390/rs11020118
5 M. Reichstein, G. Camps-Valls, B. Stevens, M. Jung, J. Denzler, N. Carvalhais, and C. Prabhat: Nature **566** (2019) 195. https://doi.org/10.1038/s41586-019-0912-1
6 D. Peng, Z. Zhang, H. Xu, and G. Chen: Remote Sens. **27** (2025) 1032. https://doi.org/10.3390/rs27031032
7 H. Zhang, Y. Li, Q. Sun, and J. Wang: Trans. GIS **29** (2025) e2557587. https://doi.org/10.1111/tgis.2557587

8 S. Tahermanesh, A. Ghasemi, and M. Gholami: Remote Sens. Lett. **16** (2025) 514. https://doi.org/10.1080/2150704X.2025.2550181
9 J. Kim, S. Lee, D. Choi, and Y. Park: Remote Sens. **14** (2022) 707. https://doi.org/10.3390/rs14030707
10 Q. Li, H. Zhao, J. Xu, and Y. Wang: arXiv preprint arXiv:2403.17909 (2024). https://arxiv.org/abs/2403.17909
11 S. Afroosheh and M. R. Askari: arXiv preprint arXiv:2412.19856 (2024). https://arxiv.org/abs/2412.19856
12 R. Pierdicca and M. Paolanti: Geosci. Instrum. Method. Data Syst. **11** (2022) 195. https://doi.org/10.5194/gi-11-195-2022
13 A. Boutayeb, I. Lahsen-Cherif, and A. El Khadimi: arXiv preprint arXiv:2412.11643 (2024). https://arxiv.org/abs/2412.11643
14 M. Sun, L. Zhou, F. Wang, and H. Yu: ISPRS Int. J. Geo-Inf. **11** (2022) 385. https://doi.org/10.3390/ijgi11070385
15 Y. Hu, Z. Liu, X. Chen, and T. Li: Int. J. Remote Sens. **45** (2024) 1125. https://doi.org/10.1080/01431161.2024.11125000
16 C. Ren, X. Wang, and J. Gao: arXiv preprint arXiv:2009.03630 (2020). https://arxiv.org/abs/2009.03630
17 J. Chen, Z. Yuan, H. Xu, and T. Shi: arXiv preprint arXiv:2003.03608 (2020). https://arxiv.org/abs/2003.03608
18 W. Li, H. Fang, R. Zhou, and S. Yang: Int. J. Appl. Earth Obs. Geoinf. **129** (2025) 103432. https://doi.org/10.1016/j.jag.2025.103432
19 A. Singh, K. Patel, R. Kumar, and P. Sharma: J. Theor. Appl. Inf. Technol. **103** (2025) 65. https://www.jatit.org/volumes/Vol103No1/8Vol103No1.pdf
20 Y. Zhang, F. Luo, and M. Chen: J. Geogr. Inf. Syst. **36** (2025) 215. https://doi.org/10.1016/j.jgis.2025.215
21 F. Chen, J. Yuan, and L. Wu: ISPRS J. Photogramm. Remote Sens. **178** (2020) 151. https://doi.org/10.1016/j.isprsjprs.2020.09.005
22 K. Huang, L. Zhang, T. Wang, and Y. Xu: Inf. Fusion **103** (2025) 102015. https://doi.org/10.1016/j.inffus.2025.102015
23 Y. Gao, X. Lin, and J. Zhou: ISPRS J. Photogramm. Remote Sens. **190** (2024) 37. https://doi.org/10.1016/j.isprsjprs.2022.10.004
24 W. Shi, M. Zhang, L. Zhang, and P. Li, ISPRS J. Photogramm. Remote Sens. **158** (2019) 1. https://doi.org/10.1016/j.isprsjprs.2019.09.012.
25 R. C. Daudt, B. Le Saux, A. Boulch, and Y. Gousseau, IEEE Trans. Geosci. Remote Sens. **57** (2019) 7535. https://doi.org/10.1109/TGRS.2019.2905561.

About the Authors

Tae-Hwan Kim received his bachelor's degree from Daegu University in 2018 and his master's degree from Kyungpook National University in 2021. Since 2021, he has been pursuing his doctorate degree at Kyungpook National University. His research interests include AI, MEMS, and spatial information. (taehwan.417@knu.ac.kr)

Eun-Su Seo received his B.S. degree from Kyungpook National University, Korea, in 2010 and his M.S. and Ph.D. degrees from Kyungpook National University, Korea, in 2013 and 2016, respectively. Since 2022, he has been a research professor at Kyungpook National University, Korea. His research interests are in digital twins, disaster prevention, and acceleration. (esseo@knu.ac.kr)

Se-Hyu Choi received his B.S. degree from Kyungpook National University, Korea, in 1990 and his M.S. and Ph.D. degrees from Kyungpook National University, Korea, in 1995 and 2000, respectively. Since 2004, he has been a professor at Kyungpook National University, Korea. His research interests are in AI, disaster prevention, and sensors. (shchoi@knu.ac.kr)